ACS APPLIED MATERIALS & INTERFACES

Research Article

www.acsami.org

In Situ Observation of Electrolyte-Concentration-Dependent Solid Electrolyte Interphase on Graphite in Dimethyl Sulfoxide

Xing-Rui Liu,[†,‡] Lin Wang,[†,‡] Li-Jun Wan,[†] and Dong Wang*[,†]

[†]CAS Key Laboratory of Molecular Nanostructure and Nanotechnology, Beijing National Laboratory for Molecular Sciences, Institute of Chemistry, Chinese Academy of Sciences, Beijing 100190, People's Republic of China

[‡]University of Chinese Academy of Sciences, Beijing 100049, People's Republic of China

Supporting Information

ABSTRACT: High lithium salt concentration strategy has been recently reported to be an effective method to enable various organic solvents as electrolyte of Li-ion batteries. Here, we utilize in situ atomic force microscopy (AFM) to investigate the interfacial morphology on the graphite electrode in dimethyl sulfoxide (DMSO)-based electrolyte of various concentrations. The significant differences in interfacial features of the graphite in electrolytes of different concentrations are revealed. In the concentrated electrolyte, stable films form primarily at the step edges and defects on the graphite surface after initial electrochemical cycling. On the other hand, in the dilute electrolyte, DMSO-solvated lithium ions constantly intercalate into graphite layers, and serious decomposition of solvent accompanied by structural deterioration of the graphite surface is observed. The in situ AFM results provide direct evidence for the concentration-dependent interface reactions between graphite electrode and DMSO-based electrolyte.

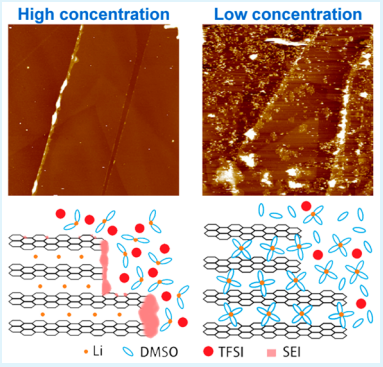

KEYWORDS: *graphite anode, dimethyl sulfoxide, solid electrolyte interphase, in situ atomic force microscopy*

INTRODUCTION

Over the past 2 decades, tremendous progress has been made in research of Li-ion batteries, especially in new cathode and anode materials. The mushrooming of the advanced electrodes put forward a higher requirement for the electrolyte, which acts as the blood of a battery. However, due to the strict requirement on the electrolyte solvents, such as ion conductivity, thermal stability, and chemical and electrochemical inertness, the development of the electrolyte is very slow and challenging.[1−3] Currently, the frequently used electrolyte solvents for Li-ion batteries are mainly ethylene carbonate (EC)-dominated organic carbonates, which show outstanding comprehensive performance of many properties.[2] Another important issue to consider for electrolyte selection is the interfacial reaction at electrode/electrolyte interface during battery operation. The mass and ion transfer at the electrode/electrolyte interface is one of the most important elementary physical chemistry processes in a battery.[4] Take graphite electrode, the most commonly used anode for its favorable reversible capacity and good cyclability,[5] as example; during the first discharging process, the reaction of the graphite with the electrolyte results in the formation of a passive film on the electrode surface, referred to as solid electrolyte interphase (SEI).[6] This passive film is a critical part for the electrochemical reactions of a graphite electrode. SEI is indispensable to ensure reversible intercalation of lithium ion into a graphite electrode to form binary lithium−graphite intercalation compounds (Li-GICs) and restrict further electrolyte decomposition to improve the cyclic performance of the electrode.[7] Obviously, the SEI-forming ability of the electrolyte is another factor to be considered for a high performance battery system.

Since the SEI is the result of electrochemical reactions between the electrolyte and the graphite electrode, its formation and properties are largely determined by the electrolyte compositions and structures.[6,8] In typical electrolytes with supporting electrolyte concentration of ca. 1 mol dm^{-3} in solvents, including EC, propylene carbonate (PC), and dimethyl sulfoxide (DMSO), Li^+ cations coordinate with solvents through ion−solvent interaction to form a Li^+-solvation-sheath structure, or solvent-separated ion pairs. The stability of the Li^+-solvation sheath is a key element in SEI growth and Li-GICs formation.[9,10] A classical scenario for the SEI formation is known as "3D mechanism" proposed by Besenhard et al.[11] In brief, solvated Li^+ intercalates into graphite layers to form a ternary GIC, and then the unstable Li^+ solvates decompose near the edges to form a passive film when the potential of graphite anode becomes reductive enough. This film would only allow dissociated Li^+ migration and hence prevent further co-intercalation of solvent molecules with Li^+ as well as electrolyte decomposition. In PC or DMSO solutions, however, the Li^+-solvation-sheath structure is more stable.[10,12] Therefore, solvated Li^+ constantly intercalates into graphite layers to form ternary solvated Li-GICs, resulting in severe exfoliation of the graphite electrode and electrolyte decom-

Received: February 3, 2015
Accepted: April 22, 2015
Published: April 22, 2015

DOI: 10.1021/acsami.5b01024
ACS Appl. Mater. Interfaces 2015, 7, 9573−9580

position instead of desirable lithium intercalation.[12,13] Thus, the electrolyte composition and solvation structure are key determinants for the interfacial reactions and electrochemical performance of graphite.

To improve the properties of the electrolyte, a simple but efficient way is using electrolyte additives. This approach could maintain the skeleton composition and structure of the electrolyte.[14−16] On the other hand, some recent results have focused on the changes of electrolyte solvation structure via varying the concentration of the dissolved lithium salt.[17−20] It has been clearly proved by Raman spectroscopy that the solvation form and ion association degree are strongly dependent on the salt concentration of the solutions.[21] Upon increasing the concentration of lithium salt, the dominant solvation structure changes from solvent-separated ion pairs to contact ion pairs or aggregates,[17] which thus affects the electrochemical reactions of electrode with electrolyte.[12] Recently, an increasing interest in developing an electrolyte system containing high concentration of lithium salt (>3 mol dm^{-3}) provides new insight into the research of better electrolytes for Li-ion batteries. When the salt concentration reaches a certain point, lithium ions are able to intercalate into the graphite layers to form the Li-GICs. This high concentration strategy universalizes the reversible lithium intercalation and deintercalation reactions at graphite in various pure solvents, such as PC, ether, nitrile, sulfoxide, or sulfone.[22−25] In the highly concentrated electrolyte, it has been suggested that almost all solvent molecules coordinate with Li^+ cations to form a structure of polymeric fluid network.[26,27] The highly concentrated electrolyte features a compromised structure between conventional electrolyte and neat ionic liquid.[1] Previously, the electrolyte concentration-dependent interface reaction process of the graphite has been investigated by a variety of characterization techniques. Nie et al. observed through ex situ TEM that the graphite particles were covered by thick films after cycling in highly concentrated PC-based electrolyte, in contrast to a thin and unstable film in dilute electrolyte.[28] Yamada et al. analyzed the surface chemical composition of the graphite electrodes after reaction in highly concentrated acetonitrile (AN) or DMSO electrolyte by ex situ XPS, suggesting that an anion-derived film formed on the graphite surface.[23,24] These results provide important insight into the concentration-dependent performance of electrolytes.

It is well-known that SEI is dynamic during the electrochemical process and sensitive to the operation conditions.[29] Thus, in situ approaches are highly desirable to understand the formation process of the SEI. In the present work, we present the morphological investigation of the SEI formation in the concentrated electrolyte via electrochemical atomic force microscopy (EC-AFM), a powerful in situ tool with high spatial resolution in the electrode/electrolyte interfacial investigation.[30−34] We used highly oriented pyrolytic graphite (HOPG) as a model for graphite electrode, and various concentrations of lithium bis(trifluoromethanesulfonyl)imide (LiTFSI) in DMSO as electrolytes. In 3.37 and 2.65 mol dm^{-3} LiTFSI/DMSO electrolyte (the molar ratio of salt and solvent is ca. 1:2 and 1:3, respectively), surface films were observed mainly at the step edges and defects on the HOPG surface, although there were some differences in the SEI formation process in the two electrolytes, whereas, in 1.0 mol dm^{-3} LiTFSI/DMSO electrolyte, continual intercalation of DMSO solvated Li^+ took place, resulting in continuous decomposition of DMSO accompanied by structural degradation of the graphite. The present results provide direct evidence for SEI formation in the concentrated electrolyte and demonstrate that the electrolyte concentration significantly affects the interfacial process and electrochemical performance of graphite electrodes.

EXPERIMENTAL SECTION

Electrolyte Preparation and Characterization. Three electrolytes of different concentrations were prepared by dissolving a given amount of LiTFSI (99.95%, Sigma-Aldrich) in pure DMSO (extra dry, 99.7+%, Acros) with stirring and heating in an argon filled glovebox. The solution structure characterization of the electrolytes was performed by Raman spectroscopy (Thermo Scientific DXR, 532 nm laser wavelength).

Natural graphite powders without any pretreatment were used for the electrochemical tests of 2.65 and 3.37 mol dm^{-3} LiTFSI/DMSO electrolytes. A natural graphite electrode was prepared by mixing natural graphite powders with 10 wt % poly(vinylidene difluoride) (PVDF) in *N*-methylpyrrolidone (NMP). The mixture was uniformly spread onto a copper current collector (99.9%) and then dried at 70 °C under vacuum overnight. Electrochemical experiments were performed using 2032-type coin cells with Li-metal foils as the counter electrodes and glass fibers (GF/D, Whatman) as separators. The charge−discharge measurements were performed on a LANHE CT2001A in the fixed voltage window between 10 mV and 2.0 V. All potentials are reported referring to Li/Li^+.

Electrochemical AFM. A freshly cleaved HOPG (ZYH type, Bruker Corp.) was used as the working electrode. In situ electrochemical AFM experiments were carried out with a commercial AFM system (Bruker Multimode 8 with a Nanoscope V controller) in a homemade argon filled glovebox at room temperature. The HOPG was mounted at the bottom of a custom designed AFM fluid cell. An external Autolab was combined with the AFM electrochemical cell to control the potential of the electrode during AFM imaging and characterize the electrochemical performance of HOPG electrodes. All AFM images were acquired in peak force tapping mode.

RESULTS

Raman Spectra of Electrolytes. The electrochemical characterization of the as-prepared electrolytes was performed by galvanostatic cycling (see the details in Supporting Information Figure S1). Raman spectra were measured to identify the solution structure of the DMSO-based electrolytes of various LiTFSI concentrations, as shown in Figure 1. In 1.0 mol dm^{-3} LiTFSI/DMSO electrolyte, two bands at 672 and 701 cm^{-1} can be assigned to C−S symmetric and asymmetric stretching modes of free DMSO, respectively.[21,23] In addition, a

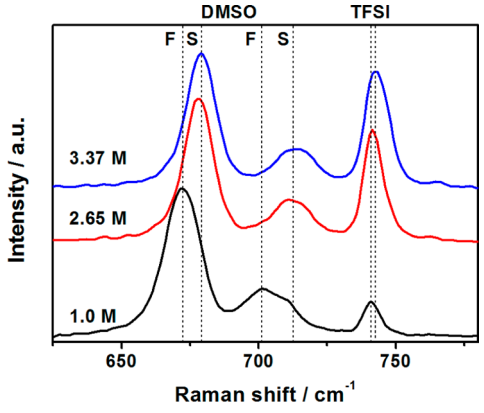

Figure 1. Raman spectra of LiTFSI/DMSO electrolytes of various salt concentrations. F indicates the Raman shift of free DMSO molecules, and S indicates the Raman shift of solvating DMSO molecules.

DOI: 10.1021/acsami.5b01024
ACS Appl. Mater. Interfaces 2015, 7, 9573−9580

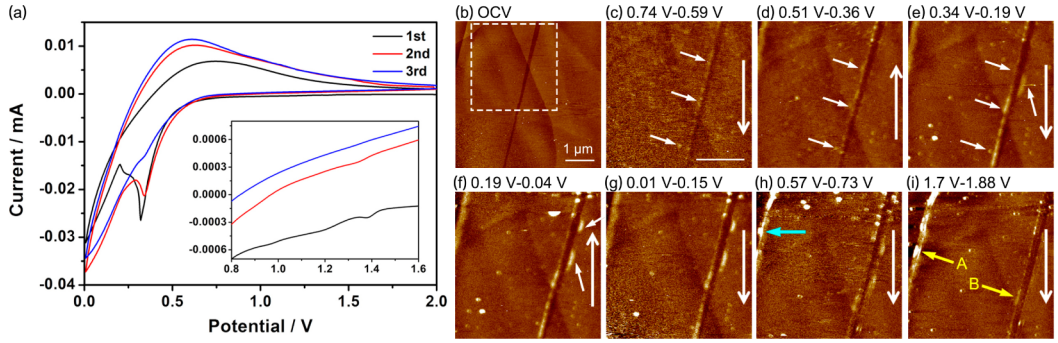

Figure 2. (a) Cyclic voltammogram of HOPG electrode in 3.37 mol dm^{-3} LiTFSI/DMSO electrolyte at a scan rate of 0.3 mV/s. The inset shows the onset of current flow above 0.8 V. (b–i) In situ AFM images of HOPG electrode in 3.37 mol dm^{-3} LiTFSI/DMSO electrolyte during the first cycle. The data scale is 4 nm. The long white arrows indicate the scan directions.

shoulder of 711 cm^{-1} in the antisymmetric C–S stretching envelope is attributed to solvating DMSO. In 2.65 and 3.37 mol dm^{-3} LiTFSI/DMSO electrolytes, the C–S symmetric band shifts toward the higher wavenumbers of 678 and 679 cm^{-1}, respectively, which are attributed to the solvating DMSO. And, the C–S asymmetric stretching peak at 713 cm^{-1} reconfirms that almost all of the solvent coordinates to Li^+ in the two concentrated solutions. It is clear from Raman results that few free DMSO molecules exist in the 2.65 and 3.37 mol dm^{-3} LiTFSI/DMSO electrolytes, while both free and solvating DMSO molecules appear in the dilute solution.[21] The Raman band of $TFSI^-$ anion shifts to higher wavenumbers in the concentrated solutions, which is caused by the formation of ion pairs between $TFSI^-$ and Li^+. What is more, the Raman shifts of DMSO and TFSI in 3.37 mol dm^{-3} LiTFSI/DMSO electrolyte are slightly larger than that in 2.65 mol dm^{-3} LiTFSI/DMSO electrolyte. It has been demonstrated that the solvation number (number of DMSO molecules coordinated to the lithium ion) decreases with increasing concentration of LiTFSI.[21] The subtle difference in the Raman spectra reflects a change in solution structure, such as solvation number and/or ion pairs, in the two concentrated solutions.

SEI Film Formation in 3.37 mol dm^{-3} LiTFSI/DMSO Electrolyte. Figure 2a shows the cyclic voltammogram of HOPG electrode in 3.37 mol dm^{-3} LiTFSI/DMSO electrolyte. In the first cycle, a major cathodic peak current begins to flow at about 0.7 V and a shoulder peak appears at around 0.25 V. A small cathodic peak around 1.4 V is observed, as shown in the inset. These peaks gradually diminish and then disappear during the subsequent cycles, suggesting that they are closely associated with the reduction reactions of the electrolyte and the formation of surface film. In addition, a large cathodic peak at potentials close to 0.01 V and a broad related anodic peak centered at about 0.6 V could be assigned to lithium intercalation and deintercalation processes, respectively.

In situ AFM was performed to obtain the morphological images of the HOPG surface during the discharging/charging cycle. Panels b–i of Figure 2 present the in situ AFM images during the first cycle. An image of HOPG at open circuit voltage (OCV) of 2.8 V (Figure 2b) shows typical structural features of HOPG basal plane, such as atomically flat terraces and several steps. The morphology remains nearly unchanged until the potential drops to below 0.74 V. Then, several particles indicated by short white arrows appear on the step edge area (Figure 2c). At potentials more negative than 0.51 V, these particles are clearly observed and their height is ca. 0.5–0.8 nm. With lowering the potential to 0.04 V, more particle-like depositions are observed on the surface and their height slowly increases to 1.5–2 nm (Figure 2e,f). During the reverse scan of potentials, the height of the particles at step B gradually reduces to around 0.8 nm, as seen in Figure 2g–i. Intriguingly, step A (marked with a cyan arrow) is covered by more deposition during the deintercalation process of lithium ions, and the thickness of the deposition is 1–10 nm. After the first cycle, the step edges are covered with thin films, and the coverage and thickness of the films are inhomogeneous at different edges.

We further investigate the morphological changes of the HOPG surface during the second cycle. Panels a–g of Figure 3

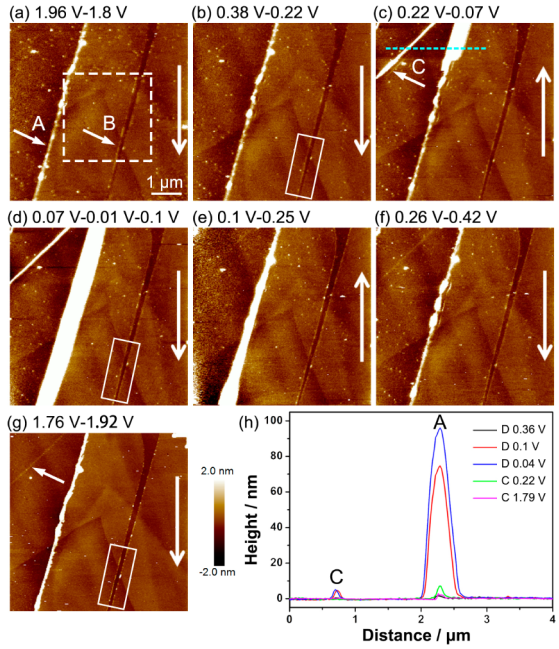

Figure 3. (a–g) In situ AFM images of HOPG electrode in 3.37 mol dm^{-3} LiTFSI/DMSO electrolyte during the second cycle. The data scale is 4 nm. The long white arrows indicate the scan directions. (h) Cross-sectional profiles of the position marked with dashed cyan line.

show in situ AFM images of the surface with enlarged scan size (the area shown in Figure 2 is marked by a white box in Figure 3a). In Figure 3a, step A and step B are covered with inhomogeneous deposition as previously described. Besides, many small particles are observed on the basal plane outside the white box, indicating that electrolyte decomposition occurred at

DOI: 10.1021/acsami.5b01024
ACS Appl. Mater. Interfaces 2015, 7, 9573–9580

the terrace in the first cycle. However, the decomposition products are not stable and can be scraped off easily during the AFM scanning.

During the discharging process from 2.0 to 0.22 V, no obvious morphological changes are observed (Figure 3b). When the potential is reduced to around 0.1 V (Figure 3c), two conspicuous swellings appear at step A and position C, which is probably a grain boundary or a wrinkle on the surface. When the delithiation process begins, the height of these swellings starts to decrease rapidly. Figure 3h presents the cross-sectional analysis of the position marked with a dashed cyan line (Figure 3c) during this cycle. The height of swelling at C is ~5 nm, while the height of swelling at A is close to 100 nm. During the charging process, the swellings rapidly subside. When the potential is more positive than 0.25 V (Figure 3e,f), the step A and feature C almost recover to their original heights. It can be inferred that the swellings might be related to the intercalation process of lithium ions.

After this process, as shown in Figure 3f, the thickness of SEI at step A has doubled (2−20 nm) in comparison to those in Figure 3a,b. When the potential is swept to 1.92 V, a more compact film covers step A and the SEI thickness is 2−23 nm (Figure 3g). In contrast, no such significant morphological changes are observed at step B, where only several inconspicuous particles of ~1 nm cover the edges, as highlighted by a white box. These results suggest that the formation of SEI during the first cycle is incomplete, and new SEI growth occurs during the lithium intercalation and deintercalation process.

SEI Film Formation in 1.0 mol dm^{-3} LiTFSI/DMSO Electrolyte. Figure 4a shows the cyclic voltammogram of HOPG in 1.0 mol dm^{-3} LiTFSI/DMSO electrolyte. During the negative sweep, several cathodic peaks are observed below the potential of 1.5 V. A bigger peak appears below 1.0 V, suggesting significant reductive reactions of the electrolyte. The cathodic current increases rapidly when the potential is more negative than 0.5 V. According to previous research,[12] the cathodic peaks in a range of 1.5−1.0 V are attributed to co-intercalation of DMSO solvents with lithium ions, and the cathodic current below 1.0 V is consistent with the reductive decomposition of the intercalated electrolyte. No anodic peaks are observed, suggesting that the electrolyte reduction is irreversible and there is no deintercalation of lithium ions from the electrode.

The morphology of the HOPG surface in dilute LiTFSI/DMSO electrolyte was investigated. Panels b−k of Figure 4 display the AFM images of HOPG in 1.0 mol dm^{-3} LiTFSI/DMSO electrolyte during the first cathodic sweep. When the potential is reduced to around 1.72 V, precipitates appear on the surface especially at the step edges and defects. And, more depositions are observed with lowering of the potentials. In addition, many flake structures, which first appear at around 1.5 V (marked by cyan arrows in Figure 4e), are present on the surface over the potential range of 1.5−1.0 V, as shown in Figure 4e−i. These flake structures change rapidly. All of the flake structures are very uniform with a height of around 0.8 nm. Previous XRD result demonstrated that when DMSO-solvated Li^+ intercalated into the graphite layers, the interlayer spacing increased by ~0.8 nm from 0.335 to 1.16 nm.[35] On the basis of the preceding morphological features, the flake structure can be attributed to the intercalation of solvated Li^+. The fast-changing surface structure directly reflects the incessant and rapid co-intercalation process. Typically, the

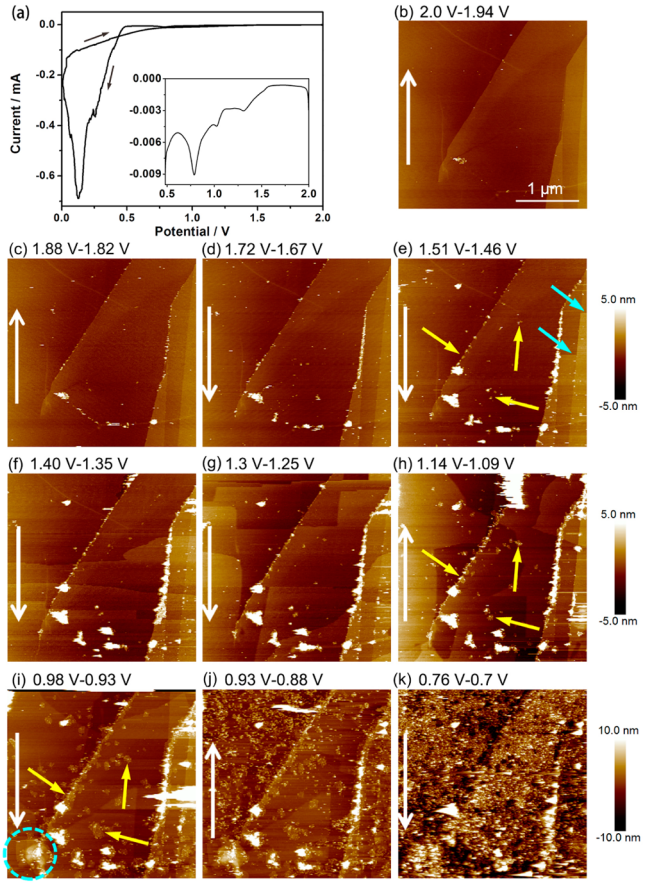

Figure 4. (a) Cyclic voltammogram of HOPG electrode in 1.0 mol dm^{-3} LiTFSI/DMSO electrolyte at a scan rate of 0.2 mV/s. The inset shows the onset of current flow above 0.5 V. (b−k) In situ AFM images of HOPG electrode in 1.0 mol dm^{-3} LiTFSI/DMSO electrolyte. The long white arrows indicate the scan directions.

intercalation of solvated Li^+ is initiated from step edges and surface defects. However, the initiation and progress of intercalation is so rapid that AFM cannot trace such a process.

Significant degradation of the HOPG surface is observed when the potential is more negative. We notice that the structural deterioration takes place around the deposition. Taking several precipitates marked with yellow arrows as examples, more and more thin deposition appears around the initial precipitates (Figure 4e−i) during the potential range of 1.5−0.93 V. And, a notable blister is observed around 0.9 V (marked by dashed cyan circle in Figure 4i). When the potential is more negative than 0.9 V, considerable decomposition of the electrolyte takes place, and the HOPG surface is totally covered with depositions (Figure 4j,k).

SEI Film Formation in 2.65 mol dm^{-3} LiTFSI/DMSO Electrolyte. We further investigate the electrochemical properties and interfacial morphology of HOPG electrode in 2.65 mol dm^{-3} LiTFSI/DMSO electrolyte during battery operation. The cyclic voltammogram of HOPG electrode in 2.65 mol dm^{-3} LiTFSI/DMSO is shown in Figure 5a. During the first cathodic sweep, two observed irreversible peaks at potentials of 1.0 and 0.4 V, respectively, could be closely related to the electrolyte reductive reactions and surface film formation. During the second cycle, the cathodic peak around 1.0 V disappears, while another peak at 0.4 V is still observable. The broad cathodic peaks at potentials below 0.2 V and the

DOI: 10.1021/acsami.5b01024
ACS Appl. Mater. Interfaces 2015, 7, 9573−9580

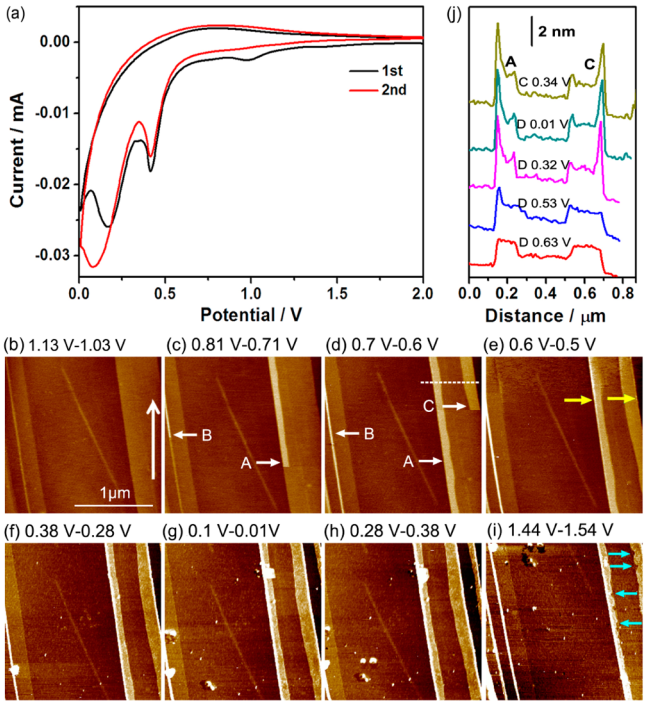

Figure 5. (a) Cyclic voltammogram of HOPG electrode in 2.65 mol dm^{-3} LiTFSI/DMSO electrolyte at a scan rate of 0.2 mV/s. (b–i) In situ AFM images of HOPG electrode in 2.65 mol dm^{-3} LiTFSI/DMSO electrolyte during the first cycle. The data scale is 4 nm. The scan directions are all from the bottom upward. (j) Cross-sectional profiles of the position marked with white dashed lines.

related anodic peaks could be assigned to intercalation and deintercalation of lithium ions, respectively.

Panels b–i of Figure 5 present the AFM images of the HOPG surface in the first cycle. During the negative sweeping, no morphological changes corresponding to the intercalation of the Li^+ solvates are observed at the potentials above 1.0 V, as shown in Figure 5b, demonstrating that the co-intercalation occurring in the dilute solution is successfully suppressed. When the potential is reduced to around 0.8 V, a narrow flake appears along step A. At the same time, the height of feature B, which is possibly a wrinkle, increases. A similar feature appears along step C, as shown in Figure 5d. According to the cross-sectional analysis (Figure 5j) of the position labeled by a white dashed line (Figure 5d), the initial height of the flakes is ~0.9 nm and their top surfaces are flat, which shows comparable features as the flake structures caused by cointercalation of DMSO-solvated Li^+ shown in Figure 4. Hence, it is inferred that the flakes are probably caused by the intercalation of some solvate species into the graphite layers through the edges or defects.[36]

When the potential is more negative than 0.52 V, these flake edges (indicated by yellow arrows) become brighter (Figure 5e–g), suggesting new substances growth. The height of the flakes almost remains unchanged during the discharging process, except for the edges and medial borders, as shown in Figure 5j. Together with the 3D images shown in Supporting Information Figure S2, it is clear that the films forming at the edges are of narrow and uniform width (~20 nm). In addition, tiny particles (~0.3 nm) are observed on the basal plane, which makes the surface look rougher (Figure 5f,g). These particles may be produced by the direct decomposition of solvent and/or salt on the HOPG surface. During the charging process, there are no significant morphological changes in the films on the edges and terrace. Nonetheless, some defects (marked by cyan arrows) appear on the medial borders of the flakes, which are possibly caused by the extraction of the intercalated species (Figure 5i).

Additionally, we investigate the morphology of the HOPG surface after the second cycle (shown in Supporting Information Figure S3). After the first cycle, almost all of the step edges are covered by passive films with height of 1–10 nm. After the second cycle, most of the films covering the edges show no significant changes, suggesting that the SEI formation in the first cycle is sound and effective in preventing further decomposition of the electrolyte.

DISCUSSION

The in situ AFM investigation on the morphological evolution of HOPG electrode revealed distinct electrode interfacial processes in DMSO-based electrolytes of three different concentrations. Table 1 summaries the interface features in the three solutions. In 3.37 mol dm^{-3} LiTFSI/DMSO electrolyte (molar ratio of LiTFSI and DMSO is ca. 1:2), no obvious co-intercalation of solvent molecules was observed during the first discharging process above 0.7 V, and an inhomogeneous film formed at the step edges at lower potentials. In 1.0 mol dm^{-3} LiTFSI/DMSO electrolyte, the amount of solvent was excessive compared with the salt. Although the step edges were covered by deposition at the potentials above 1.5 V, these precipitates were ineffective in preventing the constant co-intercalation of Li^+ solvates during the potential range of 1.5–1.0 V. In 2.65 mol dm^{-3} LiTFSI/DMSO electrolyte, where the molar ratio of LiTFSI and DMSO was ca. 1:3, sustained co-intercalation of solvent with Li^+ during 1.5–1.0 V was effectively suppressed, and only mild intercalation took place below 0.8 V. Besides, thin films forming on step edges at potential of around 0.5 V was effective in preventing further co-intercalation or decomposition of the electrolyte. The in situ AFM results confirm that increasing the salt concentration is an effective method in assisting surface SEI films formation and preventing the ceaseless intercalation of the Li^+ solvates.

Table 1. Interface Feature of HOPG Electrode in LiTFSI/DMSO Electrolytes of Different Concentrations

			interface feature	
concn (mol dm^{-3})	molality (mol kg^{-1})	molar ratio of Li and DMSO	co-intercalation	SEI
3.37	6.4	1:2	no	edge
1.0	0.9	1:14	severe (1.5–1.0 V)	basal plane
2.65	4.3	1:3	mild (<0.8 V)	edge

A model diagram shown in Figure 6 compares the differences in solution structure and interface feature in the high and low concentration electrolytes. In the concentrated solution (Figure 6a), almost all of the DMSO molecules coordinate with Li^+ and the free DMSO molecules are dramatically suppressed. At the same time, the solvation number is low and therefore the stable $Li^+(DMSO)_x$ (the optimal x = ca. 3–4) is absent in the solution.[21,37] Besides, $TFSI^-$ anions interact closely with Li^+ cations to form ion pairs. The solution structure is similar to a polymeric fluid network and completely different from that in the dilute solution. Thus, the intercalation of $Li^+(DMSO)_x$ at

DOI: 10.1021/acsami.5b01024
ACS Appl. Mater. Interfaces 2015, 7, 9573–9580

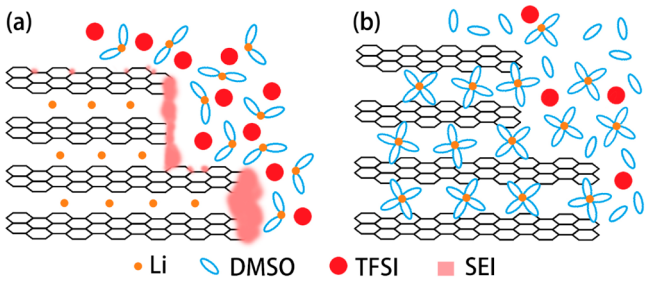

Figure 6. Model diagram of the interface reactions of the graphite electrode with highly concentrated DMSO-based electrolyte (a) and dilute DMSO-based electrolyte (b).

high potentials is successfully prevented. At lower potentials, a passive film could cover the step edges and defects, which allow for lithium ion intercalation into graphite electrode to form GICs. The polymeric fluid network structure of the electrolyte solution and formation of stable SEI both contribute to reversible discharging−charging reactions of the graphite with DMSO-based electrolyte.

In the dilute electrolyte, as shown in Figure 6b, both free DMSO molecules and stable $Li^+(DMSO)_x$ solvates exist in the solution. The $Li^+(DMSO)_x$ constantly intercalates into graphite interlayers without desolvation, resulting in the formation of a ternary Li−$(DMSO)_x$−GIC, which increases the graphite interlayer spacing by ∼0.8 nm. When the potential is more negative, continuous decomposition of electrolyte accompanied by the structural degradation takes place at a graphite electrode.

Although films formation are observed on the HOPG surface in the preceding three electrolytes of various concentrations during the first discharging process, there is an obvious difference in terms of spatial distributions of the basal plane and step edges of the HOPG surface. In the concentrated electrolyte (3.37 and 2.65 mol dm^{-3} LiTFSI/DMSO), stable films tend to form at the step edges and surface defects, as shown in Figure 6a. However, in the dilute electrolyte, many depositions appear on the basal plane even at high electrode potentials. It is generally accepted that Li^+ ions intercalate into the graphite layers only through the edges. In other words, the deposition on the basal plane is ineffective in preventing the intercalation of the Li^+ solvates. The electrolyte-concentration-dependent SEI feature suggests that different reduction reactions may occur at the edges and basal planes. In the concentrated electrolyte, free solvents are significantly suppressed. The suppression of basal plane SEI deposition in concentrated electrolyte indicates that the major reaction route on the basal plane SEI is the reduction of the solvents. As shown in the model (Figure 6a), only physisorbed particles sparsely distribute on the surface on the basal plane. The spatial resolved AFM results are consistent with the previous reports, which have suggested that basal plane SEI is mainly produced by the solvents decomposition and salt anions reduction preferentially occurs on the edges by analysis of XPS, TOF−SIMs, and other techniques.[38−41]

In addition, we notice that the SEI formation in the concentrated DMSO-based electrolyte shows different features in comparison to that in typical EC-based electrolyte at salt concentration of ca. 1 mol dm^{-3}.[36] In particular, in ca. 1 mol dm^{-3} EC-based electrolyte, it is observed that the edges and the basal plane are both covered with passive film, and the film forming on the basal plane was thicker than that in the concentrated DMSO-based electrolyte.[42,43] It is further evidenced that the decomposition of the excess solvent contributes primarily to the basal plane SEI. Generally speaking, the effective SEI on the edges of the graphite electrode is indispensible for reversible Li-ion intercalation/deintercalation, whereas the SEI on the basal plane is unfavorable as it contributes to the irreversible capacity loss. The present work indicates that the tailored SEI film on edge sites of the graphite electrode could be achieved via modulation of the electrolyte solution structure.

CONCLUSION

We investigate the SEI formation on the graphite electrode in DMSO-based electrolyte of different salt concentrations via in situ AFM. It is confirmed that electrolyte concentration significantly affects the interfacial reactions between the graphite and the DMSO-based electrolytes. In the concentrated (3.37 and 2.65 mol dm^{-3}) LiTFSI/DMSO electrolytes, constant co-intercalation of solvent with Li^+ is effectively prevented, benefiting from the unique solution structure. Besides, passive films form at the step edges and defects on the HOPG surface, allowing for reversible lithium intercalation and deintercalation at the graphite electrode. In 1.0 mol dm^{-3} LiTFSI/DMSO electrolyte, however, solvated Li^+ continuously intercalates into graphite layers, leading to serious decomposition of the electrolyte accompanied by structural deterioration of the HOPG surface. The in situ AFM investigation provides direct evidence for the surface SEI film formation in the high concentration electrolyte systems and is beneficial for the design of high performance Li-ion battery electrolyte.

ASSOCIATED CONTENT

Supporting Information

Electrochemical characterization of natural graphite electrode in 1.0, 2.65, and 3.37 mol dm^{-3} LiTFSI/DMSO electrolytes, 3D AFM images of HOPG electrode in 2.65 mol dm^{-3} LiTFSI/DMSO electrolyte, in situ AFM images of HOPG electrode in 2.65 mol dm^{-3} LiTFSI/DMSO electrolyte after the second cycle. The Supporting Information is available free of charge on the ACS Publications website at DOI: 10.1021/acsami.5b01024.

AUTHOR INFORMATION

Corresponding Author

*Fax: +86-10-62558934. E-mail: wangd@iccas.ac.cn.

Notes

The authors declare no competing financial interest.

ACKNOWLEDGMENTS

This work was supported by the Ministry of Science and Technology (Grant Nos. 2011YQ03012415, 2011CB932302, and 2011CB808701), National Natural Science Foundation of China (Grant Nos. 21127901, 21373237, and 21433011), and Strategic Priority Research Program of the Chinese Academy of Sciences (Grant No. XDB12020100).

REFERENCES

(1) Xu, K. Electrolytes and Interphases in Li-Ion Batteries and Beyond. *Chem. Rev.* **2014**, *114*, 11503−11618.
(2) Cheng, F.; Liang, J.; Tao, Z.; Chen, J. Functional Materials for Rechargeable Batteries. *Adv. Mater.* **2011**, *23*, 1695−1715.
(3) Goodenough, J. B.; Kim, Y. Challenges for Rechargeable Li Batteries. *Chem. Mater.* **2009**, *22*, 587−603.

DOI: 10.1021/acsami.5b01024
ACS Appl. Mater. Interfaces 2015, 7, 9573−9580

(4) Xu, K.; von Cresce, A. Interfacing Electrolytes with Electrodes in Li Ion Batteries. *J. Mater. Chem.* **2011**, *21*, 9849−9864.
(5) Winter, M.; Besenhard, J. O.; Spahr, M. E.; Novak, P. Insertion Electrode Materials for Rechargeable Lithium Batteries. *Adv. Mater.* **1998**, *10*, 725−763.
(6) Aurbach, D.; Markovsky, B.; Weissman, I.; Levi, E.; Ein-Eli, Y. On the Correlation between Surface Chemistry and Performance of Graphite Negative Electrodes for Li Ion Batteries. *Electrochim. Acta* **1999**, *45*, 67−86.
(7) Winter, M. The Solid Electrolyte Interphase—The Most Important and the Least Understood Solid Electrolyte in Rechargeable Li Batteries. *Z. Phys. Chem.* **2009**, *223*, 1395−1406.
(8) Nie, M.; Lucht, B. L. Role of Lithium Salt on Solid Electrolyte Interface (SEI) Formation and Structure in Lithium Ion Batteries. *J. Electrochem. Soc.* **2014**, *161*, A1001−A1006.
(9) Cazzanelli, E.; Croce, F.; Appetecchi, G. B.; Benevelli, F.; Mustarelli, P. Li^+ Solvation in Ethylene Carbonate−Propylene Carbonate Concentrated Solutions: A Comprehensive Model. *J. Chem. Phys.* **1997**, *107*, 5740−5747.
(10) Xu, K.; von Wald Cresce, A. Li^+-Solvation/Desolvation Dictates Interphasial Processes on Graphitic Anode in Li Ion Cells. *J. Mater. Res.* **2012**, *27*, 2327−2341.
(11) Besenhard, J.; Winter, M.; Yang, J.; Biberacher, W. Filming Mechanism of Lithium-Carbon Anodes in Organic and Inorganic Electrolytes. *J. Power Sources* **1995**, *54*, 228−231.
(12) Yamada, Y.; Takazawa, Y.; Miyazaki, K.; Abe, T. Electrochemical Lithium Intercalation into Graphite in Dimethyl Sulfoxide-Based Electrolytes: Effect of Solvation Structure of Lithium Ion. *J. Phys. Chem. C* **2010**, *114*, 11680−11685.
(13) Fong, R.; von Sacken, U.; Dahn, J. R. Studies of Lithium Intercalation into Carbons Using Nonaqueous Electrochemical Cells. *J. Electrochem. Soc.* **1990**, *137*, 2009−2013.
(14) Yao, W.; Zhang, Z.; Gao, J.; Li, J.; Xu, J.; Wang, Z.; Yang, Y. Vinyl Ethylene Sulfite as a New Additive in Propylene Carbonate-Based Electrolyte for Lithium Ion Batteries. *Energy Environ. Sci.* **2009**, *2*, 1102−1108.
(15) Takeuchi, S.; Fukutsuka, T.; Miyazaki, K.; Abe, T. Electrochemical Preparation of a Lithium−Graphite-Intercalation Compound in a Dimethyl Sulfoxide-Based Electrolyte Containing Calcium Ions. *Carbon* **2013**, *57*, 232−238.
(16) Zhang, S. S. A Review on Electrolyte Additives for Lithium-Ion Batteries. *J. Power Sources* **2006**, *162*, 1379−1394.
(17) Seo, D. M.; Borodin, O.; Han, S.-D.; Ly, Q.; Boyle, P. D.; Henderson, W. A. Electrolyte Solvation and Ionic Association. *J. Electrochem. Soc.* **2012**, *159*, A553−A565.
(18) McOwen, D. W.; Delp, S. A.; Paillard, E.; Herriot, C.; Han, S.-D.; Boyle, P. D.; Sommer, R. D.; Henderson, W. A. Anion Coordination Interactions in Solvates with the Lithium Salts LiDCTA and LiTDI. *J. Phys. Chem. C* **2014**, *118*, 7781−7787.
(19) Zhang, C.; Yamazaki, A.; Murai, J.; Park, J.-W.; Mandai, T.; Ueno, K.; Dokko, K.; Watanabe, M. Chelate Effects in Glyme/Lithium Bis(Trifluoromethanesulfonyl)amide Solvate Ionic Liquids, Part 2: Importance of Solvate-Structure Stability for Electrolytes of Lithium Batteries. *J. Phys. Chem. C* **2014**, *118*, 17362−17373.
(20) Cazzanelli, E.; Croce, F.; Appetecchi, G. B.; Benevelli, F.; Mustarelli, P. Li^+ Solvation in Ethylene Carbonate−Propylene Carbonate Concentrated Solutions: A Comprehensive Model. *J. Chem. Phys.* **1997**, *107*, 5740−5747.
(21) Alía, J. M.; Edwards, H. G. Ion Solvation and Ion Association in Lithium Trifluoromethanesulfonate Solutions in Three Aprotic Solvents. An FT-Raman Spectroscopic Study. *Vib. Spectrosc.* **2000**, *24*, 185−200.
(22) Suo, L.; Hu, Y.-S.; Li, H.; Armand, M.; Chen, L. A New Class of Solvent-in-Salt Electrolyte for High-Energy Rechargeable Metallic Lithium Batteries. *Nat. Commun.* **2013**, *4*, 1481−1489.
(23) Yamada, Y.; Usui, K.; Chiang, C. H.; Kikuchi, K.; Furukawa, K.; Yamada, A. General Observation of Lithium Intercalation into Graphite in Ethylene-Carbonate-Free Superconcentrated Electrolytes. *ACS Appl. Mater. Interfaces* **2014**, *6*, 10892−10899.
(24) Yamada, Y.; Furukawa, K.; Sodeyama, K.; Kikuchi, K.; Yaegashi, M.; Tateyama, Y.; Yamada, A. Unusual Stability of Acetonitrile-Based Superconcentrated Electrolytes for Fast-Charging Lithium-Ion Batteries. *J. Am. Chem. Soc.* **2014**, *136*, 5039−5046.
(25) Jeong, S.-K.; Inaba, M.; Iriyama, Y.; Abe, T.; Ogumi, Z. Interfacial Reactions between Graphite Electrodes and Propylene Carbonate-Based Solutions: Electrolyte-Concentration Dependence of Electrochemical Lithium Intercalation Reaction. *J. Power Sources* **2008**, *175*, 540−546.
(26) Sodeyama, K.; Yamada, Y.; Aikawa, K.; Yamada, A.; Tateyama, Y. Sacrificial Anion Reduction Mechanism for Electrochemical Stability Improvement in Highly Concentrated Li-Salt Electrolyte. *J. Phys. Chem. C* **2014**, *118*, 14091−14097.
(27) McOwen, D. W.; Seo, D. M.; Borodin, O.; Vatamanu, J.; Boyle, P. D.; Henderson, W. A. Concentrated Electrolytes: Decrypting Electrolyte Properties and Reassessing Al Corrosion Mechanisms. *Energy Environ. Sci.* **2014**, *7*, 416−426.
(28) Nie, M.; Abraham, D. P.; Seo, D. M.; Chen, Y.; Bose, A.; Lucht, B. L. Role of Solution Structure in Solid Electrolyte Interphase Formation on Graphite with $LiPF_6$ in Propylene Carbonate. *J. Phys. Chem. C* **2013**, *117*, 25381−25389.
(29) Verma, P.; Maire, P.; Novák, P. A Review of the Features and Analyses of the Solid Electrolyte Interphase in Li-Ion Batteries. *Electrochim. Acta* **2010**, *55*, 6332−6341.
(30) Wen, R.; Hong, M.; Byon, H. R. In Situ AFM Imaging of Li−O_2 Electrochemical Reaction on Highly Oriented Pyrolytic Graphite with Ether-Based Electrolyte. *J. Am. Chem. Soc.* **2013**, *135*, 10870−10876.
(31) Liu, R.-R.; Deng, X.; Liu, X.-R.; Yan, H.-J.; Cao, A.-M.; Wang, D. Facet Dependent Sei Formation on the $LiNi_{0.5}Mn_{1.5}O_4$ Cathode Identified by in Situ Single Particle Atomic Force Microscopy. *Chem. Commun. (Cambridge, U. K.)* **2014**, *50*, 15756−15759.
(32) Liu, X.-R.; Deng, X.; Liu, R.-R.; Yan, H.-J.; Guo, Y.-G.; Wang, D.; Wan, L.-J. Single Nanowire Electrode Electrochemistry of Silicon Anode by in Situ Atomic Force Microscopy: Solid Electrolyte Interphase Growth and Mechanical Properties. *ACS Appl. Mater. Interfaces* **2014**, *6*, 20317−20323.
(33) Inaba, M.; Jeong, S.-K.; Ogumi, Z. In Situ Scanning Probe Microscopy of Interfacial Phenomena in Batteries. *Electrochem. Soc. Interface* **2011**, *20*, 55−59.
(34) Zhang, J.; Yang, X.; Wang, R.; Dong, W.; Lu, W.; Wu, X.; Wang, X.; Li, H.; Chen, L. Influences of Additives on the Formation of a Solid Electrolyte Interphase on MnO Electrode Studied by Atomic Force Microscopy and Force Spectroscopy. *J. Phys. Chem. C* **2014**, *118*, 20756−20762.
(35) Abe, T.; Kawabata, N.; Mizutani, Y.; Inaba, M.; Ogumi, Z. Correlation between Cointercalation of Solvents and Electrochemical Intercalation of Lithium into Graphite in Propylene Carbonate Solution. *J. Electrochem. Soc.* **2003**, *150*, A257−A261.
(36) Jeong, S. K.; Inaba, M.; Abe, T.; Ogumi, Z. Surface Film Formation on Graphite Negative Electrode in Lithium-Ion Batteries: AFM Study in an Ethylene Carbonate-Based Solution. *J. Electrochem. Soc.* **2001**, *148*, A989−A993.
(37) Xuan, X.; Wang, J.; Zhao, Y.; Zhu, J. Experimental and Computational Studies on the Solvation of Lithium Tetrafluorobrate in Dimethyl Sulfoxide. *J. Raman Spectrosc.* **2007**, *38*, 865−872.
(38) Peled, E.; Golodnitsky, D.; Ulus, A.; Yufit, V. Effect of Carbon Substrate on SEI Composition and Morphology. *Electrochim. Acta* **2004**, *50*, 391−395.
(39) Chu, A. C.; Josefowicz, J. Y.; Farrington, G. C. Electrochemistry of Highly Ordered Pyrolytic Graphite Surface Film Formation Observed by Atomic Force Microscopy. *J. Electrochem. Soc.* **1997**, *144*, 4161−4169.
(40) Yan, J.; Zhang, J.; Su, Y.-C.; Zhang, X.-G.; Xia, B.-J. A Novel Perspective on the Formation of the Solid Electrolyte Interphase on the Graphite Electrode for Lithium-Ion Batteries. *Electrochim. Acta* **2010**, *55*, 1785−1794.
(41) Zhang, H.-L.; Li, F.; Liu, C.; Tan, J.; Cheng, H.-M. New Insight into the Solid Electrolyte Interphase with Use of a Focused Ion Beam. *J. Phys. Chem. B* **2005**, *109*, 22205−22211.

DOI: 10.1021/acsami.5b01024
ACS Appl. Mater. Interfaces 2015, 7, 9573−9580

(42) Deng, X.; Liu, X.-R.; Yan, H.-J.; Wang, D.; Wan, L.-J. Morphology and Modulus Evolution of Graphite Anode in Lithium Ion Battery: An in Situ AFM Investigation. *Sci. China: Chem.* **2013**, *57*, 178−183.
(43) Wang, L.; Deng, D.; Lev, L. C.; Ng, S. In-Situ Investigation of Solid-Electrolyte Interphase Formation on the Anode of Li-Ion Batteries with Atomic Force Microscopy. *J. Power Sources* **2014**, *265*, 140−148.

DOI: 10.1021/acsami.5b01024
ACS Appl. Mater. Interfaces 2015, 7, 9573−9580